



AXIS White Paper

Tracking SMBH mergers from kpc to sub-pc scales with AXIS

Adi Foord^{1,2†}, Nico Cappelluti³, Tingting Liu⁴, Marta Volonteri¹³, Melanie Habouzit, Fabio Pacucci^{5,6}, Stefano Marchesi^{10,11,12}, Nianyi Chen, Tiziana Di Matteo, Labani Mallick^{7,8,9}, Michael Koss¹⁴

¹ Department of Physics, University of Maryland Baltimore County, 1000 Hilltop Cir, Baltimore, MD 21250, USA

² Kavli Institute of Particle Astrophysics and Cosmology, Stanford University, 452 Lomita Mall, Stanford, CA 94305, USA

³ University of Miami; ncappelluti@miami.edu

⁴ Department of Physics and Astronomy, West Virginia University, P.O. Box 6315, Morgantown, WV 26506, USA

⁵ Center for Astrophysics | Harvard & Smithsonian

⁶ Black Hole Initiative at Harvard University

⁷ CITA National Fellow, University of Manitoba, Department of Physics & Astronomy, Winnipeg, Manitoba R3T 2N2, Canada

⁸ Canadian Institute for Theoretical Astrophysics, University of Toronto, 60 St George Street, Toronto, Ontario M5S 3H8, Canada

⁹ Cahill Center for Astronomy and Astrophysics, California Institute of Technology, Pasadena, CA 91125, USA

¹⁰ Dipartimento di Fisica e Astronomia (DIFA), Università di Bologna, via Gobetti 93/2, I-40129 Bologna, Italy

¹¹ Department of Physics and Astronomy, Clemson University, Kinard Lab of Physics, Clemson, SC 29634, USA

¹² INAF - Osservatorio di Astrofisica e Scienza dello Spazio di Bologna, Via Piero Gobetti, 93/3, 40129, Bologna, Italy

¹³ Institut d'Astrophysique de Paris, Sorbonne Université, CNRS, UMR 7095, 98 bis bd Arago, F-75014 Paris, France

¹⁴ Eureka Scientific, 2452 Delmer Street Suite 100, Oakland, CA 94602-3017, USA

† foord@umbc.edu

Contents

1	Introduction	2
1.1	Detecting Dual AGN	3
1.2	Detecting Binary AGN	3
2	The Power of AXIS for AGN Pair Studies	4
2.1	The Blind Search for Dual AGN in AXIS AGN Surveys	5
3	Quantifying the Rate of Dual AGN to High-z	7
4	Observations of SMBH binaries and mergers in X-rays	8
4.1	Periodicity, chirping, and merger signatures	9
4.2	Spectral hardening and double broad Fe lines	10
4.3	Synergies with other EM observatories	11

5	Population Statistics with AGN Pairs	11
5.1	Constraining Binary SMBH hardening timescales	13
5.1.1	Dual AGN	13
5.1.2	Binary AGN	13

References	13
-------------------	-----------

List of Figures

1	Dual AGN as viewed by <i>Chandra</i> and <i>AXIS</i>	5
2	Properties of Dual AGN detected by <i>AXIS</i>	6
3	The Frequency of Dual AGN Across Redshift	8
4	Binary AGN Detections with <i>AXIS</i>	10
5	Redshift versus Physical Separation for Dual AGN Detections	12

1. Introduction

Supermassive black holes (SMBHs) with masses of $10^6 - 10^9 M_{\odot}$ are ubiquitous in most massive galaxies, and classical hierarchical galaxy evolution predicts that the later stages of galaxy evolution are governed by mergers (e.g., [135]). As a result, galaxy mergers provide a favorable environment for the assembly of active galactic nuclei (AGN) pairs [131].

“Dual AGN” are pairs of AGN in the earliest phases of the galaxy merger, where the SMBHs are gravitationally unbound. They have typical separations < 30 kpc, and can sit in a single galaxy or an interacting system. The SMBHs will sink toward the center of the stellar distribution on the dynamical friction time scale. For typical values of the physical parameters governing the system (such as maximum impact parameter $b_{max} = 5$ kpc and $v \approx \sigma = 200$ km s $^{-1}$), the inspiral time is only 3 Gyr, and any $10^8 M_{\odot}$ SMBH sitting within ~ 10 kpc of the center of a typical galaxy will spiral to the center within a Hubble time. These inspiral times are expected to vary as a function of the merging environment. They may be shorter for eccentric orbits, where the SMBH can pass through higher density regions with stronger drag forces [11]; while computational analyses have shown that most minor mergers (e.g. with stellar mass ratios less than 0.1) will not result in close (< 10 kpc) SMBH pairs forming within a Hubble time [125].

The system can evolve into a SMBH binary (SMBHB), the final stage of a galaxy merger, where the two massive host galaxies have likely been interacting for hundreds of megayears to gigayears [10]. The merging system is classified as a binary when the SMBHs are gravitationally bound in a Keplerian orbit, and for a wide range SMBH masses and host galaxy environments this occurs at orbital separations < 10 pc [35,71,91]. As the last stage before coalescence, SMBHBs represent an observable link between galaxy mergers and gravitational wave (GW) events. The closest pairs (at sub-pc separations, or at $\sim 10^3 - 10^4$ Schwarzschild radii) are strong emitters of low-frequency (nHz) GWs that are expected to dominate the GW background accessible to pulsar timing arrays (PTAs; [15]), which are sensitive to massive SMBHs ($10^7 - 10^9 M_{\odot}$). They are also direct precursors to GW events detectable by future space-based laser interferometers such as the Laser Interferometer Space Antenna (LISA), which are sensitive to massive black hole (MBH) binaries with $10^4 - 10^7 M_{\odot}$ [4,88,112]. The link between pairs, binaries, and GW astrophysics, and the importance of detecting more systems is becoming increasingly stronger with recent PTA results finding evidence of a stochastic GW background consistent with a population of SMBHBs (e.g., [2,6,99,139]).

1.1. Detecting Dual AGN

Commonly measured empirical trends between the supermassive black hole mass (M) and host-galaxy bulge velocity dispersion (σ) and luminosity (L) – i.e., the M – σ and M – L relations – suggest that AGN play vital roles in shaping the properties of galaxies across cosmic time [41,57,90,92,124]. Galaxy mergers are thought to be a key process supporting the various SMBH-galaxy scaling relations [63,65,118]. Theoretically, there are many reasons to expect a link between gas-rich, similar-mass mergers and the accretion of material onto at least one of the supermassive black holes (e.g., [63,131]). Tidal forces between galaxies can introduce gravitational torques that effectively dissipate the specific angular momentum of material from the large-scale gas reservoirs and transport significant quantities down to scales in which SMBHs can accrete [5,8,29]. This can result in enhanced periods of SMBH growth, regulation of the host galaxy’s properties, and relations such as M – σ and M – L emerging (e.g., [30,138]).

However, observationally, the connection between galaxy mergers and SMBH activity remains poorly understood; various studies have found conflicting results regarding whether mergers are responsible for, or even correlated with, SMBH activity [9,37,38,51,52,54,77,98,109,110,123,126,129,134]. The activity of AGN is likely obscuration and merger-stage dependent [73,78,134]. Consequently, past measurements were likely complicated by (1) sensitivity and angular resolution of available instruments, (2) identification of galaxy mergers at high- z , and (3) intrinsic properties of merging SMBHs and their host galaxies (such as, AGN variability and gas/dust obscuration). One of the best ways to analyze the possible ties between merger environments and SMBH activity is to study systems with unique observational flags of merger-driven SMBH growth – or dual AGN. By detecting pairs of SMBHs across a wide range of redshift, we can observationally measure the role (or lack thereof) that mergers play in enhancing SMBH growth across cosmic time.

Directly detecting emission associated with two accreting SMBHs requires both angular resolution (1 kpc corresponds to angular separations less than $1''$ at $z > 0.1$) and sensitivity. Radio observations can resolve radio-emitting cores on the smallest spatial scales [28,48,49,72,93,101,104,121,136,137]; however, this technique is only efficient for the minority of AGN pairs that are expected to be radio-bright [61]. Optical selection techniques are affected by optical extinction and contamination from star formation, which is especially problematic when observing highly-obscured mergers [12,27,73,78,79,82,100,122]. As a result, the confirmation of most AGN pairs has been made via X-ray observations (e.g., NGC 6240; [75]), and most studies leverage Chandra’s superior angular resolution to discover closely-separated dual AGN [44,47,76]. However, there are less than 50 directly detected pairs of X-ray AGN candidates to date (see, e.g., [18]) as the majority of Chandra-detected dual AGN are restricted to the local universe ($z < 0.1$). High- z Chandra survey studies have resulted in non-detections [108] due to the small field of view with a high spatial resolution ($< 1.5''$) and sensitivity.

1.2. Detecting Binary AGN

Despite the strong theoretical case for the existence of SMBHBs, their observational evidence has been elusive. Currently, the only widely-accepted SMBHB is at a projected separation of 7.3 pc (in the radio galaxy 0402+379 at $z = 0.055$) where the two nuclei are directly resolved via very long baseline interferometry [101] and their proper motion is statistically significant over the course of \sim a decade [7]. However, 0402+379 is not representative of the low-frequency GW sources emitting in the PTA or LISA band, given that its separation is much wider and its GW inspiral timescale is much longer than a Hubble time. Indeed, direct observations cannot resolve the vast majority of SMBHBs in the GW-dominated regime of orbital evolution (which corresponds to \sim centi- to milli-parsec separations), and even the Event Horizon Telescope can only resolve \sim pc scales except for the most nearby systems. Therefore

the electromagnetic (EM) search for SMBHBs requires *indirect* observations from which the presence of a binary can be inferred.

Intuitively, the orbital motion of a binary may imprint on the EM emission of the system as a periodic variation of the flux. This possible binary signature has in fact been studied extensively by analytic calculations and numerical simulations, and the physical mechanisms by which an AGN hosting an SMBHB (or a “binary AGN”) can vary periodically include: BH-disk impact [64,83], modulated accretion (e.g. [33,39,53,89,97,116]), relativistic Doppler boost [34], and self-lensing [32]. Systematic searches for periodically varying AGN in large optical time-domain surveys have yielded hundreds of binary candidates (e.g. [16,19,21,55,56,84,85]), while similar searches in X-rays have been less than successful due to the pointed nature of most X-ray observations and the depth and observing cadence of current surveys (e.g., [86]). Yet, X-rays are a more direct tracer of gas in the immediate vicinity of the BHs (the so-called “minidisks”) at the inspiral stage (e.g., [24,120]), i.e., when the optical emission originates from further out in the system and may become decoupled from the binary motion (e.g., [80]). Hence, the most direct link between the growth of SMBHBs and their mergers is best established (in the EM regime) with observations at short wavelengths (especially X-rays).

In addition to tracking binary-induced periodicity, which has also been predicted in the optical bands, X-rays can *uniquely* probe signatures such as X-ray spectral hardening [40,102] and double broad Fe $K\alpha$ lines [66,113]. These signals are often accompanied by distinct emissions in other wavebands, suggesting strong synergies between an X-ray telescope and other observatories, including optical ground-based time-domain surveys such as LSST ($\sim 2025 - 2035$). More excitingly, EM observations of SMBHBs will also enable multi-messenger science in the low-frequency GW regime, which has recently been opened up by the PTA experiments (e.g., [2]). If this gravitational wave background originates from a cosmic population of SMBHBs [1], individual binaries could be detected as single sources by PTAs by ~ 2030 [68,103]. In the mid-2030s, LISA will start probing GW sources in the mHz range, among which are the mergers of massive black holes (MBHBs; $\sim 10^4 - 10^7 M_\odot$). These low-frequency GW detectors will prompt searches for EM counterparts in localized sky areas; at the same time, EM-detected SMBHBs can be used in the joint search for GW signals in PTA data or serve as “verification binaries” for LISA¹. The rich, multi-wavelength, and multi-messenger science of MBHBs and MBH mergers, therefore, demands a sensitive X-ray telescope operating at the \sim same time as the suite of EM and GW observatories in the 2030s.

2. The Power of AXIS for AGN Pair Studies

The *AXIS* point-spread-function (PSF), field-of-view (FOV), and effective area (A_{eff}) are expected to result in the detection of hundreds to thousands of new dual AGN across the redshift range $0 < z < 4$. Currently, large-scale blind searches for X-ray dual AGN are hampered by the large dependence of *Chandra*’s PSF on the off-axis angle (OAA). The shape and size of the High-resolution Mirror Assembly PSF varies significantly with source location in the telescope field-of-view, as well as the number of photons. Between $0' < \text{OAA} < 8'$, the 90% encircled energy radius grows from $\sim 2''$ to $6''$. The point spread function becomes difficult to model above OAA values of $3'$ [108], and consequently, off-axis point sources are frequently misconstrued as extended or having a multi-component structure. On top of this, putative dual AGN with angular separations $> 1''$ are difficult to detect at $\text{OAA} > 3'$, as the angular separation becomes smaller than the semi-major axis of the PSF. Although the proposed on-axis angular resolution of *AXIS* (PSF Half Energy Width = $1.25''$) is marginally larger than *Chandra*’s on-axis angular resolution

¹ X-ray observations will be crucial for identifying LISA counterparts. See *AXIS* white paper “Prospects for Time-Domain and Multi-Messenger Science with *AXIS*” for a summary of multi-messenger science with SMBHBs and the synergies of *AXIS* with low-frequency GW detectors.

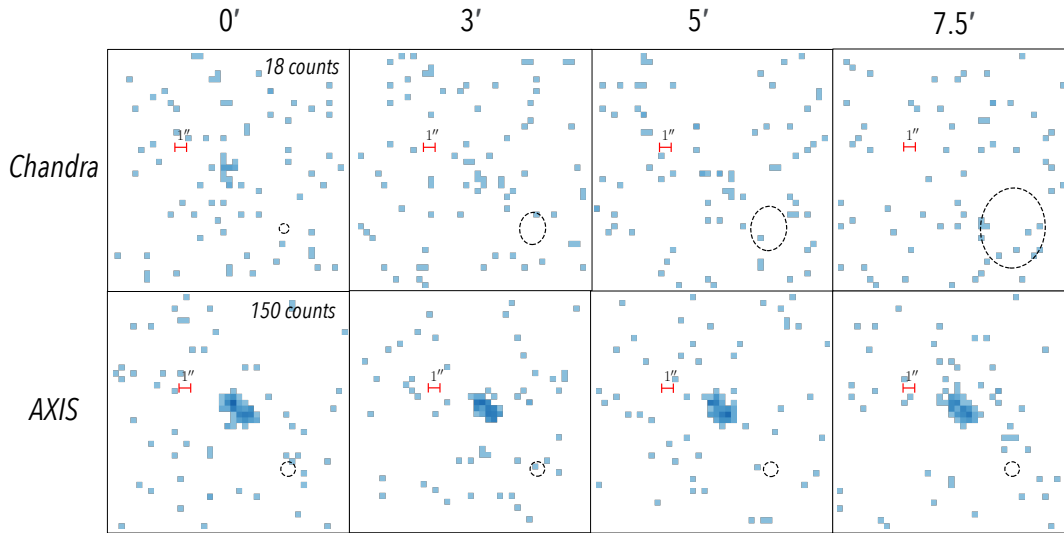


Figure 1. Dual AGN as viewed by *Chandra* and *AXIS*

A dual AGN with $L_{X, 0.5-8 \text{ keV}} = 5 \times 10^{43} \text{ erg s}^{-1}$ at $z = 3$, with $r = 1.5''$ (11.8 kpc) and a flux ratio of 0.5 (the secondary AGN has a luminosity of $L_{X, 0.5-8 \text{ keV}} = 2.5 \times 10^{43} \text{ erg s}^{-1}$). We simulate a 300 ks observation with both *Chandra* and *AXIS* as a function of increasing off-axis angle (OAA), from on-axis ($0'$) to highly off-axis ($7.5'$). On-axis, *Chandra* observes 18 counts associated with the dual AGN, while *AXIS* observes 150. We show the size of the point spread function in a black dashed line. **Given the stability of the shape and size of the *AXIS* point spread function, along with the enhanced effective area and field-of-view, a single 300 ks *AXIS* pointing results in the sensitivity to detect over $20\times$ more dual AGN than possible with a similar *Chandra* pointing.**

(PSF Half Energy Width= $0.8''$), the field-of-view average PSF is stable as a function of increasing off-axis angle ($1.5''$ up to OAA= $7.5'$) and is significantly smaller than *Chandra*'s field-of-average ($\sim 5''$ up to OAA= $7.5'$ on ACIS-I).

The *AXIS* PSF, coupled with $A_{eff, 1 \text{ keV}} = 4200 \text{ cm}^2$ and $A_{eff, 6 \text{ keV}} = 830 \text{ cm}^2$ (compared to ACIS at launch with $A_{eff, 1 \text{ keV}} = 500 \text{ cm}^2$ and $A_{eff, 6 \text{ keV}} = 200 \text{ cm}^2$), and a $24'$ diameter active field of view (compared to ACIS-I with $16'$ square field of view) will revolutionize the field of dual AGN. **A single 300 ks exposure with *AXIS* yields a sample size of 1000 AGN for which blind dual AGN searches down to $1.5''$ can be carried out. In comparison, with a 300 ks ACIS-I observation, less than 20 AGN are expected to be detected within the field that has a PSF $< 1.5''$.**

2.1. The Blind Search for Dual AGN in *AXIS* AGN Surveys

The *AXIS* AGN surveys will result in the first X-ray study that quantifies the frequency of dual AGN as a function of redshift up to $z = 3.5$. In particular, 10,000 X-ray AGN detected within a deep and intermediate survey field will yield hundreds of new dual AGN detections; including data from a serendipitous wide-area survey from Guest Observer observations could increase the detection number to the thousands. *AXIS* plans to follow a “Wedding cake” strategy to perform its extragalactic surveys: (1) a deep 5 Ms observation of a single *AXIS* pointing ($\sim 0.16 \text{ deg}^2$, or $\sim 24 \times 24$ square arcmin); and (2) an intermediate-area (2.5 deg^2) and intermediate-depth (300 ks exposure per pointing). An *AXIS* Serendipitous field built via combining Guest Observer observations (assuming 20 Ms of guaranteed non-Galactic plane time, with a median of 50 ks per pointing) could cover 50 deg^2 with a sensitivity $\sim 10^{-16} \text{ erg s}^{-1} \text{ cm}^{-2}$ (see * cite Seeding White Paper *) for more details on the surveys.

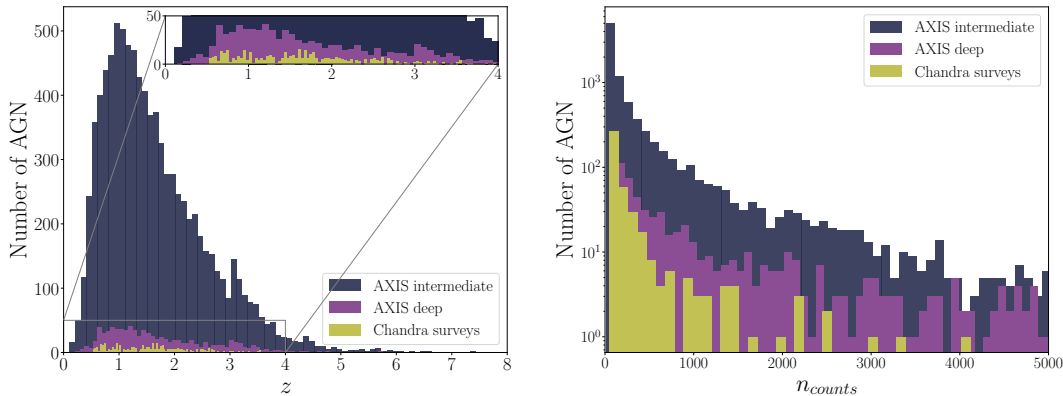


Figure 2. Properties of Dual AGN detected by *AXIS*

We show the distributions for redshift and number of 0.5–8 keV counts (n_{counts}) associated with a sample of AGN from an *AXIS* deep (5 Ms observation of a single *AXIS* pointing) and intermediate (300 ks exposure per pointing) survey from which we can analyze for the presence of a dual AGN. We include X-ray AGN that meet the following criteria: $L_{X, 0.5-8 \text{ keV}} > 10^{42} \text{ erg s}^{-1}$; n , the number of 0.5–8 keV counts, > 50 ; and $OAA < 10'$. We include z and n_{counts} information for publicly available wide and deep *Chandra* fields: X-UDS (*Chandra* imaging of the Subaru-XMM Deep/UKIDSS Ultra Deep Survey field; Kocevski et al. [74]), AEGIS-XD (*Chandra* imaging of the central region of the Extended Groth Strip; Nandra et al. [95]), CDF-S (*Chandra* Deep Field-South; Luo et al. [87]), and the COSMOS-Legacy survey (Civano et al. [23]).

We use results from end-to-end *AXIS* simulations with the SIXTE tool, as described in * cite Seeding White Paper *. Briefly, simulations have been performed using the Monte Carlo code Simulation of X-ray Telescopes (SIXTE; [25]). SIXTE simulates X-ray observations by modeling the arrival time, energy, and position of each photon based on the unique telescope input parameters (i.e., effective area, field of view, point spread function, vignetting, read-out properties, redistribution matrix). The input catalog for the *AXIS* survey simulations is based on the Gilli et al. [50] AGN population synthesis model. AGN have been simulated down to a 0.5–2 keV luminosity $L_{0.5-2} = 10^{40} \text{ erg s}^{-1}$ and up to redshift $z = 3$. In the high-redshift regime (i.e., at $z > 3$, where the AGN space density starts declining), a mock catalog built from the Vito et al. [130] $z > 3$ AGN luminosity function is used. The catalogs used are available online at <http://cxb.oas.inaf.it/mock.html> in FITS format and ready to be used within SIXTE.

From the mock *AXIS* AGN fields, we select AGN that meet the following criteria: $L_{X, 0.5-8 \text{ keV}} > 10^{42} \text{ erg s}^{-1}$; n , the number of 0.5–8 keV counts, > 50 ; and $OAA < 10'$. We imposed these cuts to form a sample of AGN where we can easily find dual AGN. For example, if $n < 50$, assuming a standard flux-ratio of ~ 0.1 [77], the secondary will be contributing < 5 X-ray counts. Our luminosity and OAA cuts follow a similar reasoning: below $10^{42} \text{ erg s}^{-1}$ we may suffer from contamination from bright X-ray binaries and/or ultra-luminous X-ray sources, and at $OAA < 10'$ the average *AXIS* PSF half energy width (HEW) is $1.5''$. After imposing these cuts, we have a sample of $\sim 10,000$ X-ray AGN. In Fig. 2, we show the distributions of z and n of our *AXIS* sample.

We compare these distributions to those for X-ray AGN from publicly available wide and deep *Chandra* fields: X-UDS (*Chandra* imaging of the Subaru-XMM Deep/UKIDSS Ultra Deep Survey field; Kocevski et al. [74]), AEGIS-XD (*Chandra* imaging of the central region of the Extended Groth Strip; Nandra et al. [95]), CDF-S (*Chandra* Deep Field-South; Luo et al. [87]), and the COSMOS-Legacy survey (Civano et al. [23]). Here, we include AGN that meet the following criteria: $L_{X, 0.5-8 \text{ keV}} > 10^{42} \text{ erg s}^{-1}$; n , the number of 0.5–8 keV counts, > 50 ; and $OAA < 4'$. In particular, the *Chandra* PSF HEW at $4'$ is close to $3''$. Between *AXIS* and *Chandra*, the samples are significantly different as a function of their size, redshift, and X-ray counts. In comparison to the 10,000 X-ray detected AGN by *AXIS*, the *Chandra* sample size is

composed of 428 AGN that span a shorter redshift range and have far fewer counts (with the majority of X-ray AGN at $z < 2.5$ and with $n_{counts} < 200$)

3. Quantifying the Rate of Dual AGN to High-z

AXIS will observationally constrain the frequency of X-ray dual AGN to within 3%, up to $z=3.5$, quantifying how (or if) mergers affect SMBH growth and galaxy evolution. If mergers play no role in enhancing SMBH growth, the expected frequency of dual AGN is predicted to be below 2% at all redshifts [3,128]; however, large-scale cosmological hydrodynamical simulations that model the physics associated with SMBH accretion and mergers and predict that the frequency of dual AGN should be a factor of two higher [17,132], while nearby observations of dual AGN predict a fraction four times as high [76]. The AXIS deep and intermediate survey will detect a sample size of AGN large enough to discern between a non-enhanced and a merger-enhanced fraction, down to angular separations of $1.5''$.

There have been many optical searches for quasar pairs in the high-redshift Universe, where tens of candidates have been identified ($z > 1$; e.g., [36,59,60,67,94]). Most recently, two of the highest- z dual AGN candidates ($z > 5$) were detected via optical spectroscopy and photometry [140,141], and new observational techniques that leverage the angular resolution of Gaia have been effective first steps for detecting the dual AGN population at high- z (i.e., [20], [22]). However, large surveys with wide-area coverage are necessary to find large samples of dual AGN candidates. A handful of large surveys in the optical regime have yielded constraints on the high- z dual AGN fraction. Silverman et al. [117] analyze double quasars resolved by the Hyper Suprime-Cam (HSC) Subaru, where ~ 100 dual AGN candidates were identified out to $z = 4.5$. Shen et al. [115] analyze 60 Gaia-resolved double quasars to measure quasar pair statistics at $z > 1.5$. Both studies find no evidence for evolution across redshift, and significantly different dual AGN fractions ($\sim 0.26 \pm 0.18\%$ vs. $\sim 6.2 \pm 0.5 \times 10^{-4} \%$). On top of this, optical selection techniques for AGN are affected by optical extinction and contamination from star formation, which is especially problematic when observing highly-obscured mergers [12,27,45,73,78,79,82,100,122].

To date, most predictions of the dual AGN fraction at high- z , and as a function of z , have been carried out via cosmological simulations [17,105,119,132].

The assumed physics, spatial and mass resolution, as well as selection criteria for dual AGN, vary across each simulation. In particular, results from the Magneticum Pathfinder Simulations (Steinborn et al. 119; box size = 182 cMpc^3) resolve SMBH pairs down to 2-5 kpc; the The Evolution and Assembly of GaLaxies and their Environment (EAGLE) simulations (Rosas-Guevara et al. 105; box size = 100 cMpc^3) resolve SMBH pairs down to 5 kpc; the Horizon-AGN simulations (Volonteri et al. 132; box size = 142 cMpc^3) resolve SMBH pairs down to 4 kpc; and ASTRID simulations (Chen et al. 17; box size = 250 cMpc^3) resolve SMBH pairs with separations down to $4/(1+z)$. Both Horizon-AGN and ASTRID include sub-grid dynamical friction modeling. A nearby observational constraint using nearby ($z < 0.05$) *Chandra* observations places a limit on spectroscopically confirmed X-ray dual AGN of $4.4^{+4.5}_{-2.2}\%$ [76], and a high- z observational constraint analyzing *Chandra* survey data at $2.5 < z < 3.5$ places an upper limit of 4.5% [108].

In Fig. 3 we plot these two observational limits, as well as results from the Horizon and ASTRID simulations [17,132]. Both the Horizon and ASTRID simulation results have been derived specifically for AXIS observations, i.e., each AGN in a pair has $L_{bo} > 10^{43}$ (Eddington-ratios down to 0.1), and all dual AGN have separations $1.5'' < r < 30 \text{ kpc}$ (via private communication). We also show the expected fraction of X-ray dual AGN, assuming the observed X-ray incidence of single AGN in galaxies [3]. We assume that each dual AGN is undergoing a galaxy merger, and weigh the X-ray incidence of a single AGN by the observed galaxy merger fraction [128] to derive the observed dual AGN fraction. Whereas the cosmological simulations include accretion physics introduced by galaxy mergers, the observed dual AGN

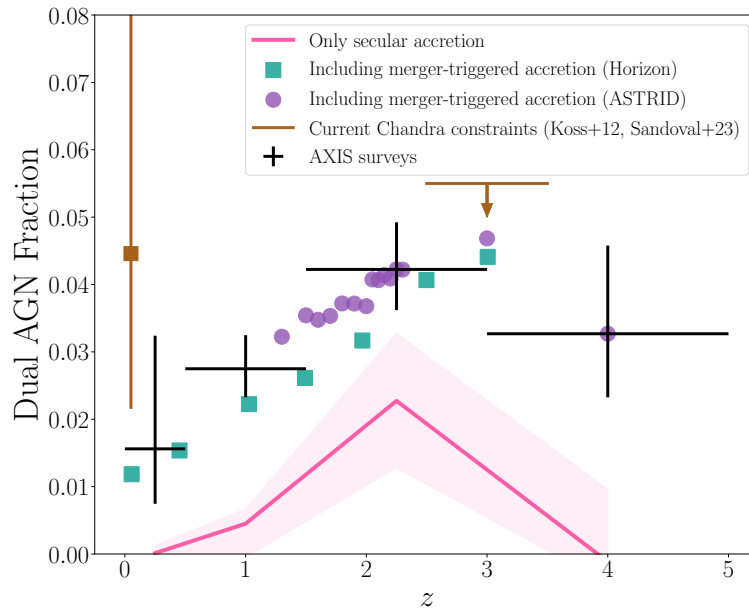


Figure 3. The Frequency of Dual AGN Across Redshift

Dual AGN fraction versus redshift. If mergers play no role in enhancing SMBH growth, we may expect the frequency of dual AGN to be under 2% at all redshifts (as estimated by the X-ray active fraction of galaxies and the observed galaxy merger rate; [3,128]). However, predictions from large-scale cosmological simulations (green squares from Horizon-AGN [132]; purple circles from ASTRID [17]) that model the physics associated with mergers and SMBH accretion predict a dual AGN fraction twice as high (between $< 1\%$ and up to 4%); and nearby observational constraints anchor the low-redshift dual AGN fraction at a factor of 4 higher (4% in the local universe). Previous X-ray analyses quantifying the dual AGN fraction at both low and high redshift (brown triangles) have resulted in non-detections and large-error bars, due to the sample size of AGN as observed by *Chandra* [78,108]. Only *AXIS* can statistically differentiate between the low- and high-end predictions and constrain the dual AGN fraction up to $z = 3.5$, measuring whether galaxy mergers enhance SMBH growth over cosmic time.

fraction represents the statistical probability of detecting two X-ray AGN in a galaxy merger, assuming that the probability of finding an X-ray AGN is not affected by the merger environment.

Using a sub-sample of 10,000 X-ray AGN from the *AXIS* survey fields (see Section 2.1), we can statistically (at the 95% C.L.) discern between predicted merger- and secular-dominated dual AGN fractions, across $0 < z < 3.5$. Interestingly, nearby observational constraints anchor the low-redshift X-ray dual AGN fraction twice as high as the merger-triggered accretion models predicated by the cosmological simulations. Assuming the X-ray dual AGN fraction scales similarly as predicted by the cosmological simulations, we may expect the X-ray dual AGN fraction to peak at values closer to 8% at $z = 2$. This would amount to detecting hundreds of more dual AGN than predicated by the cosmological simulations, and boost our population statistics.

4. Observations of SMBH binaries and mergers in X-rays

Progress over the past \sim decade on numerical simulations of an SMBH binary embedded in a circumbinary disk has drastically advanced our knowledge of its configuration, accretion mechanisms, and the expected EM output. Those simulations have reached the general consensus that the binary torque carves out an empty “cavity” in the circumbinary disk, which has a radius approximately twice

the binary separation. Nevertheless, gas flows into the cavity through narrow streams and fuels the BHs via “minidisks,” which should sufficiently power the BHs to radiate as luminously as regular AGN. This distinctive configuration, which is coupled to the binary’s orbital motion, produces a range of observational signatures that largely fall into one of two categories: variability and spectral features.

4.1. Periodicity, chirping, and merger signatures

The orbital motion of the BHs can imprint periodic variations on the EM flux of the binary system via mechanisms such as relativistic Doppler effects [34], gravitational lensing [32], modulated accretion onto the binary (e.g. [14,39,96,97]), out-flung streams of gas hitting the cavity wall [120], and mass exchange between the minidisks [13]. In the late inspiral stage where the binary orbit is rapidly shrinking, the periodicity may still be able to follow the increasing orbital frequency, producing an EM “chirp” (e.g. [120]). In order to distinguish these binary variability signatures from the more likely occurrence of regular (single) AGN variability, at least two observational requirements should be met: (1) Because of the rarity of binary AGN, a survey should probe a sufficiently large volume (i.e., sky area and depth) which samples a large number of AGN. Current observational and theoretical work puts the occurrence rate of periodically varying binaries at $\lesssim 10^{-4}$ per AGN [70,85]; detecting binary AGN would thus require a sample size of at least $\sim 10^4$ AGN. (2) Because regular AGN (powered by single BHs) are known to vary stochastically and *aperiodically*, at least a few cycles should be sampled in order to distinguish true periodicity from a stochastic process [127]. Within each cycle, the periodic variation should be tracked with a high sampling rate and high precision in order to faithfully characterize the variation and to distinguish it from stochastic variability. Thus, depending on SMBHB parameters, this corresponds to a sampling rate of \sim hours – days over a period of \sim weeks – up to decades.

There have been searches in the *Swift* BAT dataset for X-ray periodicities, with a few possible candidates [111,114]. However, past work has shown that it is challenging to distinguish true periodicity from stochastic AGN variability, especially when the measurement errors are large; and the relatively small sample size of BAT AGN ($\sim 10^3$) may not be sufficient for discovering rare binary AGN. There may be opportunities for discovery with *eROSITA* which surveys a much larger sample of AGN; however, its sampling rate may not be well-matched to the periodic timescales of the majority of SMBHBs [86]. *AXIS* will remedy both issues, through a blind search among a large number of AGN (see next section), and by targeting individual candidates to sample any periodicities with high sensitivity. Observations of these periodicities (or EM chirps) can not only identify SMBHBs, but will also enable us to study gas dynamics in extreme, time-variable spacetime and the accretion disk structure of a binary BH system, by testing the predictions of (magneto-) hydrodynamic simulations. In certain binary models, intensive monitoring over a short time period can extract even more science: for example, binary self-lensing flares encode exquisite information about the binary disk structure and even BH shadow sizes which cannot be resolved by very long baseline interferometry [26]; this can be measured by sampling \sim ten percent of the orbit at a rate that is equivalent to \sim 1 percent of the orbit.

Transient signals are also expected just prior to or shortly after the merger. For instance, in the final \sim days before coalescence, the X-ray bright minidisks shrink as the binary separation shrinks and are eventually disrupted, causing a sudden drop in X-ray flux \sim a few orbits before merger, while the optical flux, which is dominated by the outer circumbinary disk, remains steady; the system then gradually re-brightens post-merger [80]. Other simulations also show that the rapidly inspiraling binary can decouple from the circumbinary disk which may also cause a sharp decline in flux at short wavelengths [31]. The synergy here with an optical survey like LSST is clear: the candidate can be identified by the sudden disappearance of its X-ray flux accompanied by a steady optical emission. More importantly, this signature

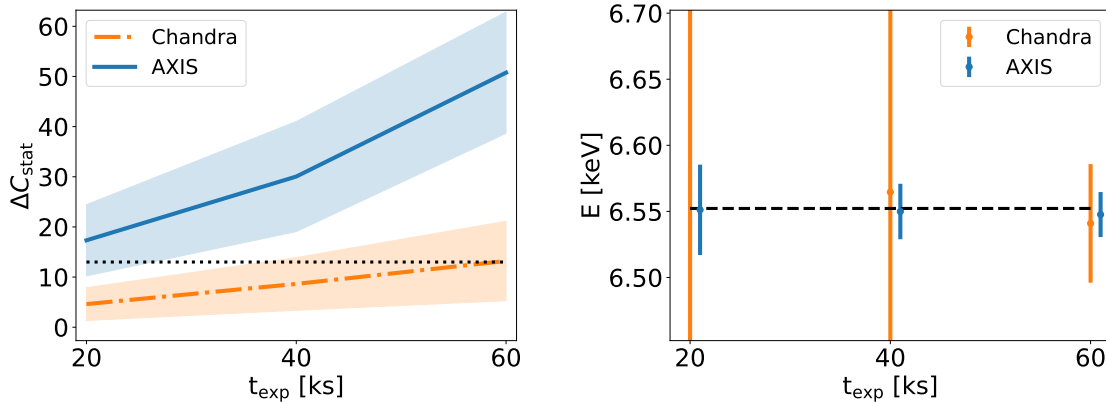


Figure 4. Binary AGN Detections with *AXIS*

We simulate a mock binary AGN with two broad iron lines separated by 0.4 keV which corresponds to a $10^9 M_{\odot}$ SMBHB at a sub-pc separation. The same spectrum is observed with *Chandra* and *AXIS* with 20 ks, 40 ks, and 60 ks exposure. Left panel: a more positive ΔC_{stat} indicates that the double-line model is statistically favored. The colored bands correspond to the respective 1σ distributions. For comparison purposes, the dotted line marks a nominal detection threshold which corresponds to the approximate ΔC_{stat} achieved with a 60 ks *Chandra* observation, below which the double iron line model is not favored at high confidence. Right panel: The energy of the second line recovered by spectral fitting as a function of exposure time. (The dashed line marks the true value.) *Chandra* is unable to constrain its energy with 20 or 40 ks observations (consistent with the marginal detections shown on the left); however, *AXIS* can constrain the parameter to high precision with only 20 ks.

can, in principle, be identified with as few as two observations [80] and could be the “smoking gun” signature of an MBHB approaching merger.

4.2. Spectral hardening and double broad Fe lines

As the accretion streams strike the minidisks, shock-heating produces bright X-ray emission in excess of the conventional power-law X-ray spectrum of an AGN [40,102]. This spectral hardening signature may be distinguished by searching for excess luminosity in the X-ray energy range or modeling the AGN X-ray spectrum, as in previous studies of individual sources with *Chandra* and *NuSTAR* [43,46,106,107]. [81] predicts that the all-sky number of sources which exhibit this signature is $\sim 10^2$ at the 10^{-13} erg cm $^{-2}$ s $^{-1}$ flux level, or $\sim 10^4$ for sources that are ~ 100 times fainter. Thus, identifying this type of binary signature in blind searches is feasible with the large number of AGN after combining the dedicated *AXIS* surveys and serendipitous observations. The depth in the latter, serendipitous field will reach $\sim 10^{-16}$ erg s $^{-1}$ cm $^{-2}$ in an ~ 50 deg 2 sky area [ref], thus potentially yielding a large number of SMBHBs that display this signature.

Additionally, X-ray signatures of a binary may also originate from the minidisks themselves which produce fluorescent Fe $K\alpha$ lines. The line energies are expected to be Doppler shifted in opposite directions as the result of radial velocity changes, producing a double broad Fe line feature which periodically oscillates with time [66,113]. A past study with *Swift* XRT has revealed tantalizing evidence for such a signature [114]; however, since the spectrum was effectively integrated over a significant fraction of the putative binary period, the temporal information is lost. With *AXIS*’ large effective area at 6 keV (830 cm 2), a double Fe line feature in a similar source could be distinguished from noise fluctuations in a “snapshot” observation (and ideally, its oscillation would be captured over several visits per orbit). Meanwhile, resolving this broad line feature only requires a moderate energy resolution at 6 keV (~ 0.1 keV), which is easily met by *AXIS*. Figure 4 shows an example where distinguishing between double- and single-line

models at the same statistical significance level requires ~ 60 ks exposure with *Chandra*, but only ~ 20 ks with *AXIS*. Similarly, *AXIS* is able to recover the energy of the second line with high precision, thereby constraining the physical parameters of the system; by contrast, *Chandra* would require three times the exposure time to achieve a comparable precision level.

4.3. Synergies with other EM observatories

Those X-ray emissions from binaries are usually accompanied by signatures at UV, optical, and infrared wavelengths, offering opportunities to probe the same SMBHB source across the EM spectrum. For instance, theory predicts that excess X-ray emission can be produced by streams crossing the cavity and striking the minidisks; the same cavity is expected to cause a deficit in the UV due to the missing gas (e.g. [102]). Other examples can be found in the wavelength-dependent variability amplitudes or patterns (or achromaticity) predicted by binary models (e.g. [32,34,133]). In fact, not only are multi-wavelength observations beneficial for the studies of SMBHBs; they are *necessary* in order to robustly distinguish binaries because of the high occurrence rates of interlopers (namely, regular AGN). Therefore, an X-ray telescope will be a powerful arbitrator of SMBHB candidates discovered by other facilities in other wavebands, in addition to a potentially powerful discovery engine on its own. For example, a number of studies have been carried out with *Chandra*, *XMM* or *NuSTAR* to observe the X-ray spectra and search for the predicted X-ray excess, or other peculiar features, for a sample of SMBHB candidates that display possible optical periodicity selected from ground-based time-domain surveys (e.g. [43,46,106]). In ~ 2032 , the Rubin Observatory LSST will be well into its ten-year operation and potentially will have discovered \sim a dozen to \sim a hundred periodically varying SMBHBs [69,70]. A similar follow-up study with an X-ray telescope such as *AXIS* will examine the nature of these periodic sources and place stringent tests on their binary hypothesis.

5. Population Statistics with AGN Pairs

The majority of dual AGN detected by *AXIS* will span physical separations below 20 kpc, a physical regime where merger-induced effects are believed to be important to the SMBH growth [62]. In the nearby universe ($z = 0.1$), *AXIS* is capable of detecting dual AGN at $L_X > 10^{41}$ erg s^{-1} at $r < 5$ kpc; at $z = 2$ *AXIS* is capable of detecting dual AGN at $L_X > 10^{42}$ erg s^{-1} down to $r = 12$ kpc; and at $z > 5$ *AXIS* is capable of detecting dual AGN down to physical separations $r > 10$ kpc. Assuming the dual AGN fraction follows predictions from cosmological simulations, we expect the deep and intermediate *AXIS* survey to detect ~ 200 dual AGN between $0 < z < 4$. **This detection sample is over a magnitude more than the expected dual AGN detections from publicly available *Chandra* fields (~ 10), assuming similar luminosity and X-ray count thresholds.**

In Fig. 5 we show distributions for redshift and physical separation associated with a mock sample of dual AGN from an *AXIS* deep (5 Ms observation of a single *AXIS* pointing) and intermediate (300 ks exposure per pointing) survey. We include redshift and physical separations for a mock sample of dual AGN detected via publicly available wide and deep *Chandra* fields (see Fig. 2). Assuming the dual AGN fraction follows predictions from cosmological simulations, we create a mock subsample of dual AGN in each redshift bin with $L_X > 10^{40}$ erg s^{-1} . We assign a physical separation to each dual AGN, sampling from a distribution of physical separations measured for X-ray dual AGN in the nearby universe [76]. We note that our ability to detect dual AGN in a given *AXIS* observation can be amplified using available statistical tools. In particular, tools such as BAYMAX [42,44,47] can push analyses to angular separations $\sim 0.8''$ across a wide range of flux ratios, corresponding to a physical separation $r < 7$ kpc at $z = 1.6$ (where the angular diameter distance peaks).

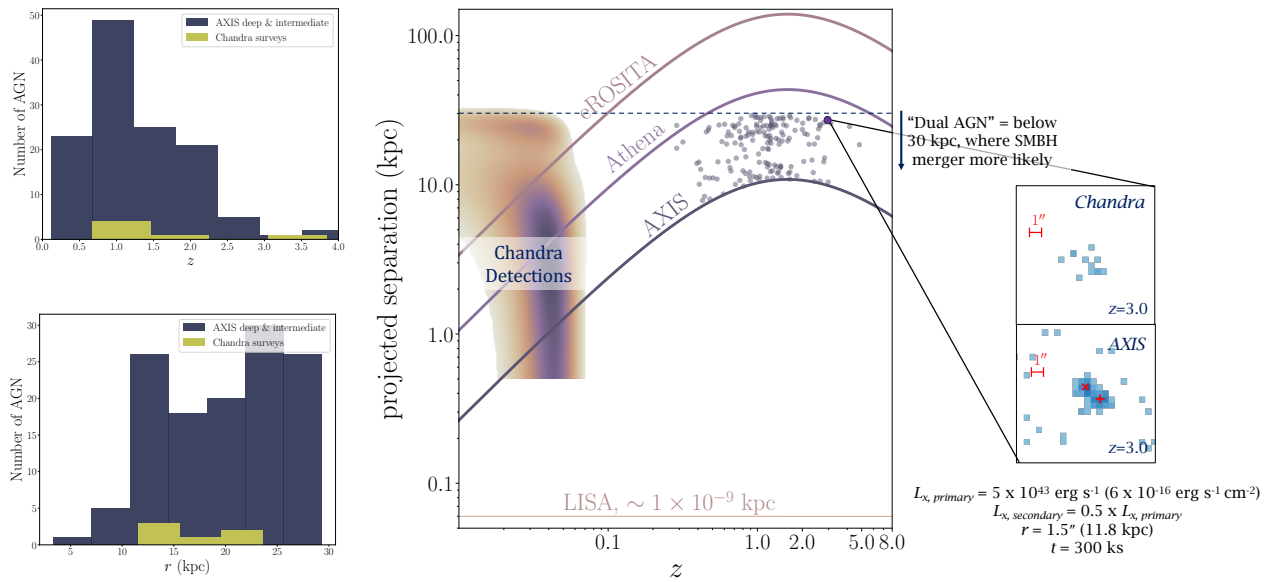


Figure 5. Redshift versus Physical Separation for Dual AGN Detections

Distributions for redshift and physical separation associated with a mock sample of dual AGN from an *AXIS* deep (5 Ms observation of a single *AXIS* pointing) and intermediate (300 ks exposure per pointing) survey. We include redshift and physical separations for a mock sample of dual AGN detected via publicly available wide and deep *Chandra* fields (see Fig. 2). Assuming the dual AGN fraction follows predictions from cosmological simulations, we create a mock subsample of dual AGN in each redshift bin. We assign a physical separation to each dual AGN, sampling from a distribution of physical separations measured for X-ray dual AGN in the nearby universe [76]. For *AXIS*, a dual AGN is detected if the angular separation is larger than $1.25''$, while for *Chandra*, a dual AGN is detected if the angular separation is larger than $0.8''$.

5.1. Constraining Binary SMBH hardening timescales

5.1.1. Dual AGN

Most recently, results from PTAs such as NANOGrav have found evidence for a GW background (GW frequencies between \sim nHz and 100 nHz), with oscillations of \sim months to \sim a decade [2]. The GW signal has been compared to simulations of various SMBH binary populations, and based on current measurements, the amplitude of the signal suggests that SMBHs may be (1) more common or (2) more massive than previously thought. An important component in breaking this degeneracy is a strong constraint on the overall SMBH hardening timescale. In particular, the final signal of binaries detected by PTAs is driven by mergers occurring at $z = 0.3 - 0.8$, which correlate with progenitor dual AGN at < 30 kpc-scale separations at $z = 1 - 3$ (see fig. 12 in Agazie et al. [1]). Thus, constraining the frequency of dual AGN detections at $z = 1 - 3$, as a function of separation, will make a big impact on future binary SMBH model inferences. In Fig. 5 we show current dual AGN detections from *Chandra*, which are mostly constrained to the nearby universe, and expected dual AGN detections by *AXIS*. In particular, *AXIS* will detect some of the highest-redshift dual AGN to date, over a large range of physical separations.

5.1.2. Binary AGN

The discovery of \sim a few dozen SMBHBs at different orbital periods would provide an indirect test of their hardening timescales [58]. In the GW-driven regime, the residence timescale $t_{\text{res}} = t_{\text{GW}} = -R/(dR/dt)$ is the time a binary spends at a given separation R , or equivalently, the corresponding orbital period t_{orb} , and scales with the period: $t_{\text{GW}} \propto t_{\text{orb}}^{8/3}$. Since the number of binaries at a given orbital period is determined by the probability of observing them at this stage: $N \propto (t_{\text{res}}/t_{\text{Q}})$, where $t_{\text{Q}} \sim 10^7$ yr is the typical quasar lifetime, this yields a simple scaling relation between the fraction of sources and their periods in the GW regime: $f \propto t_{\text{orb}}^{8/3}$. Hence, with a sample of SMBHBs whose orbital periods are measured from, e.g., EM periodicity, one can test the steep, $t_{\text{orb}}^{8/3}$ scaling relation due to GW inspiral. By contrast, a shallower scaling relation would probe the timescale due to gas interactions.

Acknowledgments: We kindly acknowledge the *AXIS* team for their outstanding scientific and technical work over the past year. This work is the result of several months of discussion in the *AXIS*-AGN SWG. AF thanks Stanford University for support during the proposal writing phase.

1. Agazie, G., Anumalapudi, A., Archibald, A. M., et al. 2023, *ApJ*, 952, L37
2. —. 2023, *ApJ*, 951, L8
3. Aird, J., Coil, A. L., & Georgakakis, A. 2019, *MNRAS*, 484, 4360
4. Amaro-Seoane, P., Andrews, J., Arca Sedda, M., et al. 2023, *Living Reviews in Relativity*, 26, 2
5. Anglés-Alcázar, D., Davé, R., Faucher-Giguère, C.-A., Özel, F., & Hopkins, P. F. 2017, *MNRAS*, 464, 2840
6. Antoniadis, J., Arumugam, P., Arumugam, S., et al. 2023, *arXiv e-prints*, arXiv:2306.16214
7. Bansal, K., Taylor, G. B., Peck, A. B., Zavala, R. T., & Romani, R. W. 2017, *ApJ*, 843, 14
8. Barnes, J. E., & Hernquist, L. E. 1991, *ApJ*, 370, L65
9. Barrows, R. S., Comerford, J. M., & Greene, J. E. 2018, *ApJ*, 869, 154
10. Begelman, M. C., Blandford, R. D., & Rees, M. J. 1980, *Nature*, 287, 307
11. Binney, J., & Tremaine, S. 1987, *Galactic dynamics*
12. Blecha, L., Snyder, G. F., Satyapal, S., & Ellison, S. L. 2018, *MNRAS*, 478, 3056
13. Bowen, D. B., Campanelli, M., Krolik, J. H., Mewes, V., & Noble, S. C. 2017, *ApJ*, 838, 42
14. Bowen, D. B., Mewes, V., Noble, S. C., et al. 2019, *ApJ*, 879, 76
15. Burke-Spolaor, S., Taylor, S. R., Charisi, M., et al. 2019, *A&A Rev.*, 27, 5
16. Charisi, M., Bartos, I., Haiman, Z., et al. 2016, *MNRAS*, 463, 2145
17. Chen, N., Di Matteo, T., Ni, Y., et al. 2023, *MNRAS*, 522, 1895

18. Chen, Y.-C., Hwang, H.-C., Shen, Y., et al. 2022, *ApJ*, 925, 162
19. Chen, Y.-C., Liu, X., Liao, W.-T., et al. 2020, *MNRAS*, 499, 2245
20. Chen, Y.-C., Liu, X., Foord, A., et al. 2023, *Nature*, 616, 45
21. Chen, Y.-J., Zhai, S., Liu, J.-R., et al. 2022, *arXiv e-prints*, arXiv:2206.11497
22. Ciurlo, A., Campbell, R. D., Morris, M. R., et al. 2020, *Nature*, 577, 337
23. Civano, F., Marchesi, S., Comastri, A., et al. 2016, *The Astrophysical Journal*, 819, 62
24. d'Ascoli, S., Noble, S. C., Bowen, D. B., et al. 2018, *ApJ*, 865, 140
25. Dauser, T., Falkner, S., Lorenz, M., et al. 2019, *A&A*, 630, A66
26. Davelaar, J., & Haiman, Z. 2022, *Ph. Rev. D*, 105, 103010
27. De Rosa, A., Vignali, C., Husemann, B., et al. 2018, *MNRAS*, 480, 1639
28. Deane, R. P., Paragi, Z., Jarvis, M. J., et al. 2014, *Nature*, 511, 57
29. Di Matteo, T., Colberg, J., Springel, V., Hernquist, L., & Sijacki, D. 2008, *ApJ*, 676, 33
30. Di Matteo, T., Springel, V., & Hernquist, L. 2005, *Nature*, 433, 604
31. Dittmann, A. J., Ryan, G., & Miller, M. C. 2023, *ApJ*, 949, L30
32. D'Orazio, D. J., & Di Stefano, R. 2018, *MNRAS*, 474, 2975
33. D'Orazio, D. J., Haiman, Z., & MacFadyen, A. 2013, *MNRAS*, 436, 2997
34. D'Orazio, D. J., Haiman, Z., & Schiminovich, D. 2015, *Nature*, 525, 351
35. Dotti, M., Colpi, M., Haardt, F., & Mayer, L. 2007, *MNRAS*, 379, 956
36. Eftekharzadeh, S., Myers, A. D., Hennawi, J. F., et al. 2017, *MNRAS*, 468, 77
37. Ellison, S. L., Patton, D. R., Mendel, J. T., & Scudder, J. M. 2011, *MNRAS*, 418, 2043
38. Fan, L., Han, Y., Fang, G., et al. 2016, *ApJ*, 822, L32
39. Farris, B. D., Duffell, P., MacFadyen, A. I., & Haiman, Z. 2014, *ApJ*, 783, 134
40. —. 2015, *MNRAS*, 446, L36
41. Ferrarese, L., & Merritt, D. 2000, *ApJ*, 539, L9
42. Foord, A., Gültekin, K., Nevin, R., et al. 2020, *ApJ*, 892, 29
43. Foord, A., Gültekin, K., Reynolds, M., et al. 2017, *ApJ*, 851, 106
44. Foord, A., Gültekin, K., Runnoe, J. C., & Koss, M. J. 2021, *ApJ*, 907, 71
45. —. 2021, *ApJ*, 907, 72
46. Foord, A., Liu, X., Gültekin, K., et al. 2022, *ApJ*, 927, 3
47. Foord, A., Gültekin, K., Reynolds, M. T., et al. 2019, *ApJ*, 877, 17
48. Fu, H., Myers, A. D., Djorgovski, S. G., et al. 2015, *ApJ*, 799, 72
49. Gabányi, K. É., Frey, S., Xiao, T., et al. 2014, *MNRAS*, 443, 1509
50. Gilli, R., Comastri, A., & Hasinger, G. 2007, *A&A*, 463, 79
51. Glikman, E., Simmons, B., Mailly, M., et al. 2015, *ApJ*, 806, 218
52. Glikman, E., Lacy, M., LaMassa, S., et al. 2018, *ApJ*, 861, 37
53. Gold, R., Paschalidis, V., Etienne, Z. B., Shapiro, S. L., & Pfeiffer, H. P. 2014, *Ph. Rev. D*, 89, 064060
54. Goulding, A. D., Greene, J. E., Bezanson, R., et al. 2018, *Publications of the Astronomical Society of Japan*, 70, S37
55. Graham, M. J., Djorgovski, S. G., Stern, D., et al. 2015, *Nature*, 518, 74
56. —. 2015, *MNRAS*, 453, 1562
57. Gültekin, K., Richstone, D. O., Gebhardt, K., et al. 2009, *ApJ*, 698, 198
58. Haiman, Z., Kocsis, B., & Menou, K. 2009, *ApJ*, 700, 1952
59. Hennawi, J. F., Strauss, M. A., Oguri, M., et al. 2006, *AJ*, 131, 1
60. Hennawi, J. F., Myers, A. D., Shen, Y., et al. 2010, *ApJ*, 719, 1672
61. Hooper, E. J., Impey, C. D., Foltz, C. B., & Hewett, P. C. 1995, *ApJ*, 445, 62
62. Hopkins, P. F., Bundy, K., Hernquist, L., & Ellis, R. S. 2007, *ApJ*, 659, 976
63. Hopkins, P. F., Hernquist, L., Cox, T. J., et al. 2006, *ApJS*, 163, 1
64. Ivanov, P. B., Igumenshchev, I. V., & Novikov, I. D. 1998, *ApJ*, 507, 131
65. Jahnke, K., & Macciò, A. V. 2011, *ApJ*, 734, 92
66. Jovanović, P., Borka Jovanović, V., Borka, D., & Bogdanović, T. 2014, *Advances in Space Research*, 54, 1448

67. Kayo, I., & Oguri, M. 2012, *MNRAS*, 424, 1363
68. Kelley, L. Z., Blecha, L., Hernquist, L., Sesana, A., & Taylor, S. R. 2018, *MNRAS*, 477, 964
69. Kelley, L. Z., D’Orazio, D. J., & Di Stefano, R. 2021, *MNRAS*, 508, 2524
70. Kelley, L. Z., Haiman, Z., Sesana, A., & Hernquist, L. 2019, *MNRAS*, 485, 1579
71. Khan, F. M., Berentzen, I., Berczik, P., et al. 2012, *ApJ*, 756, 30
72. Kharb, P., Lal, D. V., & Merritt, D. 2017, *Nature Astronomy*, 1, 727
73. Kocevski, D. D., Brightman, M., Nandra, K., et al. 2015, *ApJ*, 814, 104
74. Kocevski, D. D., Hasinger, G., Brightman, M., et al. 2018, *The Astrophysical Journal Supplement Series*, 236, 48
75. Komossa, S., Burwitz, V., Hasinger, G., et al. 2003, *ApJ*, 582, L15
76. Koss, M., Mushotzky, R., Treister, E., et al. 2012, *ApJ*, 746, L22
77. Koss, M., Mushotzky, R., Veilleux, S., & Winter, L. 2010, *ApJ*, 716, L125
78. Koss, M. J., Assef, R., Baloković, M., et al. 2016, *ApJ*, 825, 85
79. Koss, M. J., Blecha, L., Bernhard, P., et al. 2018, *Nature*, 563, 214
80. Krauth, L. M., Davelaar, J., Haiman, Z., et al. 2023, *arXiv e-prints*, arXiv:2304.02575
81. Krolik, J. H., Volonteri, M., Dubois, Y., & Devriendt, J. 2019, *ApJ*, 879, 110
82. Lanzuisi, G., Civano, F., Marchesi, S., et al. 2018, *MNRAS*, 480, 2578
83. Lehto, H. J., & Valtonen, M. J. 1996, *ApJ*, 460, 207
84. Liu, T., Gezari, S., Heinis, S., et al. 2015, *ApJ*, 803, L16
85. Liu, T., Gezari, S., Ayers, M., et al. 2019, *ApJ*, 884, 36
86. Liu, T., Koss, M., Blecha, L., et al. 2020, *ApJ*, 896, 122
87. Luo, B., Brandt, W. N., Xue, Y. Q., et al. 2016, *The Astrophysical Journal Supplement Series*, 228, 2
88. Luo, J., Chen, L.-S., Duan, H.-Z., et al. 2016, *Classical and Quantum Gravity*, 33, 035010
89. MacFadyen, A. I., & Milosavljević, M. 2008, *ApJ*, 672, 83
90. Magorrian, J., Tremaine, S., Richstone, D., et al. 1998, *AJ*, 115, 2285
91. Mayer, L., Kazantzidis, S., Madau, P., et al. 2007, *Science*, 316, 1874
92. McConnell, N. J., & Ma, C.-P. 2013, *ApJ*, 764, 184
93. Müller-Sánchez, F., Comerford, J. M., Nevin, R., et al. 2015, *ApJ*, 813, 103
94. Myers, A. D., Richards, G. T., Brunner, R. J., et al. 2008, *ApJ*, 678, 635
95. Nandra, K., Laird, E. S., Aird, J. A., et al. 2015, *The Astrophysical Journal Supplement Series*, 220, 10
96. Noble, S. C., Krolik, J. H., Campanelli, M., et al. 2021, *ApJ*, 922, 175
97. Noble, S. C., Mundim, B. C., Nakano, H., et al. 2012, *ApJ*, 755, 51
98. Onoue, M., Kashikawa, N., Uchiyama, H., et al. 2018, *PASJ*, 70, S31
99. Reardon, D. J., Zic, A., Shannon, R. M., et al. 2023, *arXiv e-prints*, arXiv:2306.16215
100. Ricci, C., Bauer, F. E., Treister, E., et al. 2017, *MNRAS*, 468, 1273
101. Rodriguez, C., Taylor, G. B., Zavala, R. T., et al. 2006, *ApJ*, 646, 49
102. Roedig, C., Krolik, J. H., & Miller, M. C. 2014, *ApJ*, 785, 115
103. Rosado, P. A., Sesana, A., & Gair, J. 2015, *MNRAS*, 451, 2417
104. Rosario, D. J., Shields, G. A., Taylor, G. B., Salviander, S., & Smith, K. L. 2010, *ApJ*, 716, 131
105. Rosas-Guevara, Y. M., Bower, R. G., McAlpine, S., Bonoli, S., & Tissera, P. B. 2019, *MNRAS*, 483, 2712
106. Saade, M. L., Stern, D., Brightman, M., et al. 2020, *ApJ*, 900, 148
107. Saade, M. L., Brightman, M., Stern, D., et al. 2023, *arXiv e-prints*, arXiv:2304.06144
108. Sandoval, B., Foord, A., Allen, S. W., & Stemo, A. in prep.
109. Satyapal, S., Ellison, S. L., McAlpine, W., et al. 2014, *MNRAS*, 441, 1297
110. Schawinski, K., Simmons, B. D., Urry, C. M., Treister, E., & Glikman, E. 2012, *MNRAS*, 425, L61
111. Serafinelli, R., Severgnini, P., Braitto, V., et al. 2020, *ApJ*, 902, 10
112. Sesana, A., Haardt, F., & Madau, P. 2007, *ApJ*, 660, 546
113. Sesana, A., Roedig, C., Reynolds, M. T., & Dotti, M. 2012, *MNRAS*, 420, 860
114. Severgnini, P., Ciccone, C., Della Ceca, R., et al. 2018, *MNRAS*, 479, 3804
115. Shen, Y., Hwang, H.-C., Oguri, M., et al. 2023, *ApJ*, 943, 38

116. Shi, J.-M., Krolik, J. H., Lubow, S. H., & Hawley, J. F. 2012, [ApJ](#), 749, 118
117. Silverman, J. D., Tang, S., Lee, K.-G., et al. 2020, [ApJ](#), 899, 154
118. Sobral, D., Stroe, A., Dawson, W. A., et al. 2015, [MNRAS](#), 450, 630
119. Steinborn, L. K., Dolag, K., Comerford, J. M., et al. 2016, [MNRAS](#), 458, 1013
120. Tang, Y., Haiman, Z., & MacFadyen, A. 2018, [MNRAS](#), 476, 2249
121. Tingay, S. J., & Wayth, R. B. 2011, [AJ](#), 141, 174
122. Torres-Albà, N., Iwasawa, K., Díaz-Santos, T., et al. 2018, [A&A](#), 620, A140
123. Treister, E., Schawinski, K., Urry, C. M., & Simmons, B. D. 2012, [ApJ](#), 758, L39
124. Tremaine, S., Gebhardt, K., Bender, R., et al. 2002, [ApJ](#), 574, 740
125. Tremmel, M., Governato, F., Volonteri, M., Quinn, T. R., & Pontzen, A. 2018, [MNRAS](#), 475, 4967
126. Urrutia, T., Lacy, M., & Becker, R. H. 2008, [ApJ](#), 674, 80
127. Vaughan, S., Uttley, P., Markowitz, A. G., et al. 2016, [MNRAS](#), 461, 3145
128. Ventou, E., Contini, T., Bouché, N., et al. 2017, [A&A](#), 608, A9
129. Villforth, C., Hamann, F., Rosario, D. J., et al. 2014, [MNRAS](#), 439, 3342
130. Vito, F., Gilli, R., Vignali, C., et al. 2014, [MNRAS](#), 445, 3557
131. Volonteri, M., Haardt, F., & Madau, P. 2003, [ApJ](#), 582, 559
132. Volonteri, M., Pfister, H., Beckmann, R., et al. 2022, [MNRAS](#), 514, 640
133. Westernacher-Schneider, J. R., Zrake, J., MacFadyen, A., & Haiman, Z. 2022, [Ph. Rev. D](#), 106, 103010
134. Weston, M. E., McIntosh, D. H., Brodwin, M., et al. 2017, [MNRAS](#), 464, 3882
135. White, S. D. M., & Rees, M. J. 1978, [MNRAS](#), 183, 341
136. Wrobel, J. M., Comerford, J. M., & Middelberg, E. 2014, [ApJ](#), 782, 116
137. Wrobel, J. M., Walker, R. C., & Fu, H. 2014, [ApJ](#), 792, L8
138. Wyithe, J. S. B., & Loeb, A. 2003, [ApJ](#), 595, 614
139. Xu, H., Chen, S., Guo, Y., et al. 2023, [arXiv e-prints](#), arXiv:2306.16216
140. Yue, M., Fan, X., Yang, J., & Wang, F. 2021, [ApJ](#), 921, L27
141. —. 2023, [AJ](#), 165, 191